Journal of Hydrology 584 (2020) 124668

Contents lists available at ScienceDirect

Journal of Hydrology

journal homepage: www.elsevier.com/locate/jhydrol

Research papers

Seasonal stratification of a deep, high-altitude, dimictic lake: Nam Co, Tibetan Plateau

Junbo Wang[a,b,*], Lei Huang[a], Jianting Ju[a], Gerhard Daut[c], Qingfeng Ma[a], Liping Zhu[a,b], Torsten Haberzettl[c,d], Jussi Baade[c], Roland Mäusbacher[c], Andrew Hamilton[e], Kelly Graves[e], Jason Olsthoorn[e], Bernard E. Laval[e]

[a] Key Laboratory of Tibetan Environment Changes and Land Surface Processes (TEL) /Nam Co Observation and Research Station (NAMORS), Institute of Tibetan Plateau Research, Chinese Academy of Sciences, Beijing 100101, China
[b] CAS Center for Excellence in Tibetan Plateau Earth Sciences, Beijing 100101, China
[c] Institute of Geography, Friedrich-Schiller-University Jena, 07743 Jena, Germany
[d] Physical Geography, Institute of Geography and Geology, University of Greifswald, 17489 Greifswald, Germany
[e] Department of Civil Engineering, University of British Columbia, Vancouver, BC V6T 1Z4, Canada

ARTICLE INFO

This manuscript was handled by Marco Borga, Editor-in-Chief, with the assistance of Marco Toffolon, Associate Editor

Keywords:
Nam Co
The Tibetan Plateau
Radiatively driven convection
Winter stratification
Dimictic
Thermal fluxes

ABSTRACT

We investigate the seasonal evolution of stratification in a deep (100 m), high-altitude (4,730 m a.s.l.) dimictic lake on the Tibetan Plateau using three years of observation of Nam Co. The lake is situated at relatively low latitude (30 °N) where it receives high solar radiative forcing (observed maximum daily average 400 W m^{-2}), yet the annual average air temperature is close to 0 °C at this high altitude. These features make Nam Co distinct from most well-documented dimictic lakes, which are usually located at higher latitude and lower altitude. We classify seasonal stratification into six phases based on strength of stratification, surface temperature relative to the temperature of maximum density, ice-cover, and heat and mixing dynamics, which we use to compare Nam Co with better-documented, higher-latitude dimictic lakes. While the three warm stratification phases (i.e. when water is warmer than the temperature of maximum density) in Nam Co are relatively cold, they are otherwise similar to that observed in high-latitude dimictic lakes. Conversely, two of Nam Co's cold stratification phases are distinct from that reported in high-latitude lakes. These two phases are characterized by the interplay between the relatively strong radiative forcing and surface heat flux, and include the following: 1) during fall turnover, persistent winds aided by radiatively driven convection prolong vertical mixing (i.e. turnover) and surface heat loss such that the entire water column cools well below the temperature of maximum density (as low as 1 °C); and 2) in contrast, under ice-cover with relatively little snow, the entire water column of the lake warms continuously due to through-ice solar radiative flux. The intense cooling and heating during these two phases counteract each other such that hypolimnetic temperature at spring turnover is similar to that observed in high latitude lakes. Our observations highlight the relative importance of radiatively driven convection on the seasonal stratification dynamics of Nam Co, and underscore that these dynamics must be considered when attempting to predict climate change impacts on high-altitude, low-latitude lakes, including the > 1100, largely unstudied, lakes on the Tibetan Plateau.

1. Introduction

The seasonal cycle of thermal stratification in large, deep freshwater lakes is modified by latitude and altitude (MacIntyre and Melack, 2009). In general, annual average air temperature decreases with both increasing latitude and altitude, thus the effect of increasing altitude on lake stratification is typically assumed to be equivalent to increasing latitude (e.g., Hutchison and Löffler, 1956; Lewis, 1983). While this generalized latitude/altitude equivalency captures variation in bulk heat input, it neglects changes to the components of surface heat flux with changing latitude. In particular, it overlooks latitudinal changes of penetrating solar radiation versus non-penetrating heat fluxes (net long wave radiation, sensible and latent heat). This is significant because, when fresh water is colder than the temperature of maximum density

* Corresponding author at: Key Laboratory of Tibetan Environment Changes and Land Surface Processes (TEL) /Nam Co Observation and Research Station (NAMORS), Institute of Tibetan Plateau Research, Chinese Academy of Sciences, Beijing 100101, China.
E-mail address: wangjb@itpcas.ac.cn (J. Wang).

https://doi.org/10.1016/j.jhydrol.2020.124668
Received 23 October 2019; Received in revised form 23 January 2020; Accepted 7 February 2020
Available online 08 February 2020
0022-1694/

(T_{md} ~ 4 °C for pure water at standard atmospheric pressure) warming increases density, and penetrating solar radiation drives convection within the water column (c.f. Farmer, 1975; Mironov et al., 2002).

In "typical" (e.g. high latitude, low altitude) dimictic lakes, radiatively driven convection is only significant during the later stages of winter, when solar radiation is strong but ice cover persists, with minimal snow cover (e.g. Winter II as defined by Kirillin et al., 2012). Conversely, radiatively driven convection is typically considered insignificant during the ice-free season between fall turnover and ice-formation because fall turnover occurs near the annual solar minimum (e.g. Farmer and Carmack, 1981). For example, at 60 °C latitude, top-of-atmosphere, daily-average solar radiative forcing varies from a maximum of 350 W m^{-2} during summer solstice, to a minimum of 25 W m^{-2} during winter solstice around the time of fall turnover (e.g. Pawlowicz et al., 2001). Radiatively driven convection is also considered insignificant during early winter because of continued low solar radiation at that time combined with snow attenuation and reflection (e.g. Winter I; Kirillin et al., 2012).

To highlight latitudinal versus altitudinal effects on penetrating versus non-penetrating heat fluxes, consider that global annual-average surface air temperature at 30 °N is 20 °C (Peixoto and Oort, 1992), yet due to its high elevation the annual average air temperature on the Tibetan Plateau is ~0 °C (You et al., 2007), more comparable to global annual temperatures at 60 °N. Conversely, the annual *minimum* top-of-atmosphere solar insolation at 30° latitude is 220 W m^{-2}, substantially more than the 25 W m^{-2} annual minimum at 60° latitude (Pawlowicz et al., 2001). Thus, lakes at the altitude and latitude of the Tibetan Plateau are subjected to low winter air temperatures comparable to lakes at 60° N, but with much stronger solar forcing.

The Tibetan Plateau is a large, distinct, and relatively understudied geographic region. Its high mean elevation (~4000 m a.s.l.) results in low air temperature despite its relatively low latitude (Qiu, 2008). More than 1123 lakes larger than 1 km^2, with a combined surface area of 4×10^4 km^2, are distributed across the Tibetan Plateau (Zhang et al., 2013), making it a globally significant lake region. Though the authors do not get into energetics analyses, published observations of thermistor chain data from Bangong Co (Wang et al., 2014) and Nam Co (Wang et al., 2019) show that fall isothermal cooling extends well below T_{md}, suggesting either strong wind stirring or an additional mixing mechanism not typically considered important at fall overturn (e.g. radiatively driven convection). In addition, their data show both lakes warmed isothermally under ice-cover suggesting Winter II conditions (Kirillin et al., 2012) prevailed during the ice-covered period.

In this paper we explore the effects of low air temperature and high solar forcing on seasonal stratification, emphasizing turnover and winter stratification when lake water is colder than the temperature of maximum density. We present three years of observations of thermal stratification in Nam Co, a large, deep high-altitude lake on the central Tibetan Plateau, based on continuous *in situ* monitoring. We develop a heat budget to validate heat flux estimates, then quantify energetics of mixing and stratification to identify six distinct phases of the seasonal evolution of thermal stratification, which are shown to be controlled by a competition between combined mixing effects due to wind and the seasonally alternating mixing and stratifying effects of surface buoyancy flux. The six phases of seasonal stratification observed in Nam Co are then discussed in relation to observations of seasonal stratification of comparator lakes.

2. Materials and methods

2.1. Site description

Nam Co (lake center at 30° 40′N, 90° 30′E) is a dimictic, endorheic lake at high altitude (4730 m a.s.l.) located in the central part of the Tibetan Plateau (Fig. 1a; Wang et al., 2019). The lake has a surface area of 2020 km^2 making it the third largest lake in the Tibetan Plateau region (Zhang et al, 2013). The basin shape is dominated by a large, flat deep-water area in the central part of the lake, where the water depth is generally > 95 m, and the maximum recorded water depth is 98.9 m. A small shallower sub-basin exists to the east of Kunduo and Qiduo islands (Fig. 1c), with a maximum water depth of ~60 m (Wang et al., 2009). The lake volume is estimated as 86 km^3 and has been increasing over several decades (Zhu et al., 2010).

Climatically, Nam Co is located in the monsoon-influenced transition zone between semi-humid and semi-arid areas. The mean annual wind speed is 4 m s^{-1} with a maximum monthly mean wind speed of 6.1 m s^{-1} occurring in January (You et al., 2007). The Nam Co area has an annual mean air temperature of approximately 0 °C, and precipitation of ~450 mm a^{-1} (Guan et al., 1984; Ma et al., 2012), with distinct rainy and dry seasons. The precipitation during the warm rainy season (May-September) constitutes 91% of the total annual precipitation (Guan et al., 1984; Ma et al., 2012). Some attempts have been made to estimate the annual evaporation from Nam Co's surface, with a range of values reported (635 mm (Ma et al., 2016); 658 mm (Haginoya et al., 2009); 832 ± 69 mm (Lazhu et al., 2016)).

River inflow into the lake primarily occurs during the summer season, with mean summer flow rates 200–300 m^3 s^{-1}, yielding a seasonal lake level increase of 400–1000 mm (Zhou et al., 2013). Zhou et al. (2013) conducted a water balance for Nam Co during the open water months (May – October) and found a consistent imbalance over five years that they attribute to net groundwater recharge from Nam Co 100 – 200 m^3 s^{-1}. Assuming this outflow is constant year-round gives a hydraulic residence time 10–15 years. This long residence time suggests the influence of inflows on seasonal timescales is insignificant to heat budgets and stratification, and inflows will be assumed negligible in this work.

As expected for an endorheic lake, Nam Co is saline and alkaline. Measured specific conductivity and pH are 1850 μS cm^{-1} and 9.2, respectively (Wang et al., 2009), with Na^+ and HCO_3^- the dominant cation and anion in the lake water, respectively. Wang et al. (2010) showed that an evaporation-crystallization process is the main controlling mechanism of the lake water chemistry. As will be shown, the observed salinity distribution is of secondary importance to the seasonal evolution of thermal stratification except during spring melt of ice and snow.

Based on remote sensing (MODIS) data and in-situ observations, Gou et al. (2017) found that complete freezing and start of break-up in Nam Co occurred in late January and mid-late April, respectively, with an average complete ice cover period of ~80 days. Also based on remote sensing, Cai et al. (2019) reported the mean breakup end date at Nam Co was 9th, May. The thickest ice is observed in mid-March with a thickness of ~60 cm based on the in-situ measurement.

2.2. Field data

Meteorological data (air temperature, precipitation, wind speed, short- and long-wave radiation) were recorded at 10-minute intervals at the Nam Co station (Fig. 1c) with a Vaisala MIRO520 automated weather station.

Temperature data loggers (VEMCO Minilog-II-T, Canada; accuracy: ± 0.1 °C from −5 to 35 °C; resolution: 0.01 °C), were deployed throughout the entire study period at station T2 (Fig. 1c) from late October 2011 to early July 2014 at the following depths: 6, 16, 21, 26, 31, 36, 56 and 66 m. A logger at 46 m depth was lost, and the loggers at 21 and 31 m depth were deployed in May 2013. The logging interval was 10 min. Two CTD90M multi-parameter probes (Sea & Sun Technology, Germany) measuring *in situ* temperature, electrical conductivity, pressure, and turbidity were deployed near the surface (~3 m deep, late May 2012 to middle September 2013) and the bottom (~83 m deep, late May 2012 to early July 2014) of the mooring at station T2 with a recording interval of 2 h. Unfortunately, the 83 m turbidity sensor became fouled in January 2013, giving high turbidity

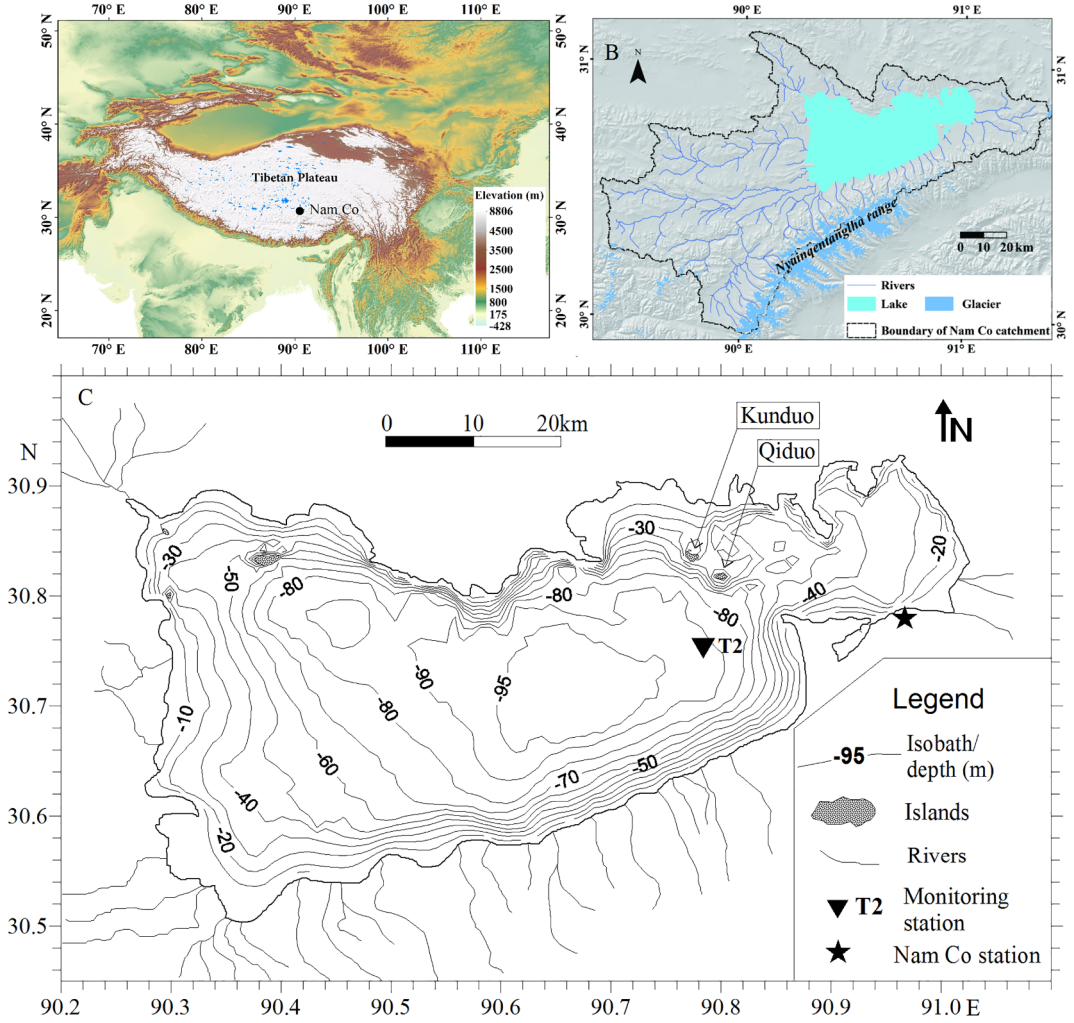

Fig. 1. Map of study site. a) location of Nam Co within the Tibetan Plateau. b) Nam Co catchment showing major tributaries and glaciated regions. c) Nam Co bathymetry showing the location of the monitoring station T2, and the Nam Co station. The islands Kunduo and Qiduo separate the Main Basin of Nam Co to the west from the Eastern Basin.

values (~40 FTU), which decreased to < 1 FTU upon servicing. Thus, these data are not shown.

Regular water quality profiling of *in situ* temperature, specific conductivity and photosynthetically active radiation (PAR) was conducted with a multi-parameter sonde (Hach Hydrolab DS5, USA) at one station in the main western basin (T2, ~93 m depth; Fig. 1c) every two to four weeks from early April to late November, covering most of the open water period. The Hydrolab conductivity and temperature sensors were calibrated at 1–2 year intervals and spot-checked against the two moored CTD90M multi-parameter probes. One profile was made at T2 with a CTD90M multi-parameter probe on 8 September 2013 and *in situ* temperature, specific conductivity and turbidity are presented here.

Direct measurements of ice-thickness were made offshore of the peninsula to the southeast of Qiduo Island (Fig. 1c).

Following Pawlowicz (2008) *in situ* salinity is calculated from *in situ* C_{25} using a site-specific linear relation derived from the chemical analysis of water samples in Wang et al. (2010). A linear fit through the narrow range of water sample C_{25} (1880–2250 μS cm^{-1}) is given by

$$S = 1\text{g } L^{-1}(mScm^{-1})^{-1}C_{25} - 0.35 \text{ g } L^{-1}, \quad (1)$$

and has an R^2 value of 0.99. *In situ* C_{25} measurements from CTD profiles presented here range from 1.7 to 1.9 mS cm^{-1}, which is slightly outside the range Eq. (1) is based on. Given the high R^2 for Eq. (1), we use Eq. (1) for this work on the assumption that even extrapolated to 1.7 mS cm^{-1} Eq. (1) is more accurate than a fit forced through zero. This choice of regression versus one forced through zero does not change the overall conclusions. Water density was calculated as σ_0 (i.e. sigma-0, density calculated using *in situ* temperature and salinity with atmospheric pressure minus 1000 kg m^{-3}) using the thermodynamic equation of state (TEOS-10; Pawlowicz and Feistel, 2012).

2.3. Remote sensing

The evolution of snow and ice-cover during the field study was observed from daily repeat Terra/MODIS corrected reflectance true-colour image mosaics downloaded from NASA WorldView [https://worldview.earthdata.nasa.gov]. For ice-cover categorization purposes the lake was divided into two regions, the Eastern Basin (east of islands Kunduo and Qiduo) and the Main Basin (west of islands Kunduo and Qiduo; Fig. 1c). Snow and ice-cover were identified manually as 'none', 'partial', or 'complete' for each region each day. Dates when the lake was obscured by cloud cover were neglected, so the total days of snow cover may be underestimated.

2.4. Surface heat flux

A heat budget was calculated from available meteorological and radiation data measured at Nam Co station (Fig. 1c) combined with bulk heat transfer models. Due to the relatively long hydraulic residence time (10–15 years), heat flux due to surface and ground water

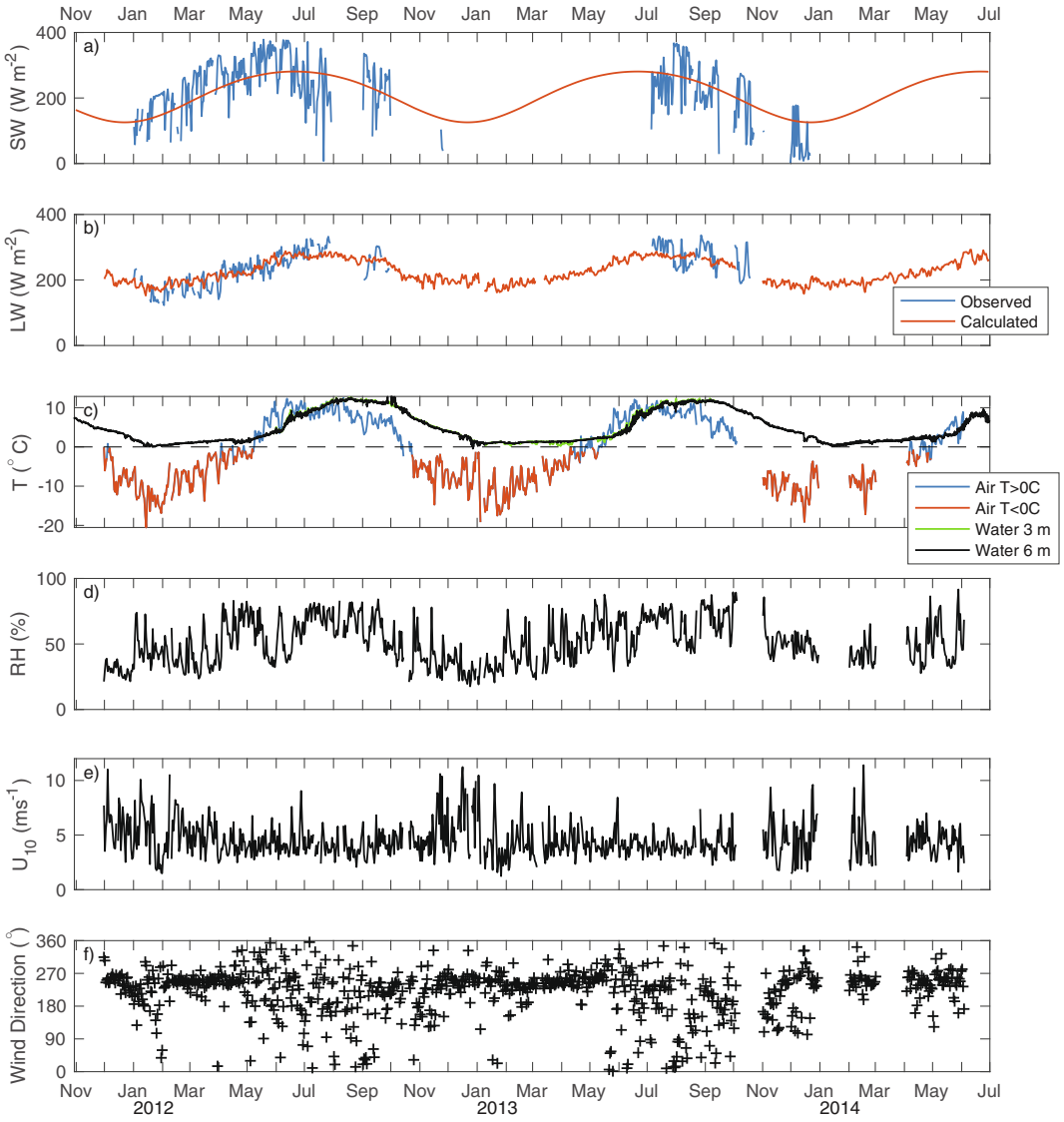

Fig. 2. Daily average meteorological observations measured at Nam Co Station, 1.6 m above ground. a) Observations of downwelling shortwave radiation are compared with values estimated using top of atmosphere calculations with a calibrated constant atmospheric transmissivity. Values are corrected for lake water albedo. b) Observations of downwelling longwave radiation are compared with bulk thermodynamic relations using air temperature measured at Nam Co station and a calibrated constant cloud cover coefficient. c) Air and lake water temperature. d) Relative humidity. e) Wind speed scaled to 10 m above ground. f) Wind direction.

inflows and outflows were neglected. Bengsston et al. (1996) observed sediment heat flux under-ice of ~1 W m^{-2} in shallow (1–10 m) regions of lakes. Given the large depth of Nam Co (mean depth of 42 m), sediment heat flux is unlikely to contribute significantly to the heat budget and is neglected in this analysis. Only surface short- and longwave radiative, sensible and latent heat flux as detailed below are considered in the heat budget.

2.4.1. Penetrative heat flux

Downwelling short wave radiation measured at Nam Co station was not available for the entire monitoring period. To extend available data to cover the entire period, mean atmospheric transmission was estimated as 62% from the average of the ratio of available data to top of atmosphere calculations for downwelling solar radiation (Payne, 1972). Predicted downwelling shortwave radiation at the lake surface was then estimated by multiplying predicted top of atmosphere downwelling solar radiation by the mean atmospheric transmission estimated above. A comparison of observed and predicted downwelling shortwave radiation at the lake surface is given in Fig. 2a. While day-to-day fluctuations due to cloud cover are not captured by the prediction, the mean annual trend is. Shortwave radiation albedo for open water was calculated using Payne (1972).

During periods of complete ice-cover, penetrating shortwave radiation is assumed to be the dominant component of surface heat flux and other heat fluxes (e.g. net longwave, sensible and latent heat) are neglected. The satellite-based visual-band imagery discussed above suggests that other than cracking and rifting, ice-cover is clear with very little white ice, and that snow cover on the ice is episodic and short-lived. Ice-cover albedo was considered for the following two conditions: no or partial snow cover; or complete snow cover. Following Perovich (1991) ice albedo was taken as 0.4, (roughly consistent with the spectral average of clear-ice albedo) for days with no or partial snow cover (Table 1), and 0.8 (roughly consistent with ice-covered by new snow) for days with complete snow cover. Attenuation of shortwave radiation by propagation through ice-cover was accounted for using a clear-ice extinction coefficient of 1.5 m^{-1} (Launiainen and Cheng, 1998) applied to the mean observed ice thickness of 0.55 m. Given the lack of snow depth or snow properties, extinction of shortwave radiation propagating through snow was not considered. As will be shown, the estimated shortwave radiative heat flux closely matches

Table 1
Total number of days of ice and snow cover on Nam Co during the three years of observation. Estimates were made using MODIS corrected reflectance true colour imagery downloaded from NASA Worldview (https://worldview.earthdata.nasa.gov/).

	2011–2012	2012–2013	2013–2014
Ice-cover Starts	5 Jan 2012	22 Dec 2012	21 Dec 2013
Ice-cover Complete	30 Jan 2012	24 Jan 2013	29 Jan 2014
Open Water Starts	30 Mar 2012	6 May 2013	14 Apr 2014
Open Water Complete	13 May 2012	23 May 2013	18 May 2014
Partial Snow Cover (days)	23	24	32
Complete Snow Cover (days)	7	69	28

the observed heating rate of Nam Co under ice cover validating our simple model and crude approximations for the optical properties of snow and ice.

2.4.2. Non-penetrative heat fluxes

Available observed downwelling longwave radiation was compared with calculations from the bulk formulae of Swinbank (1963) based on observed air temperature (Fig. 2b). The mean square difference between observations and calculations was minimized for a cloud cover of 40%. Constant cloud cover misses day-to-day variability as well as some seasonal variability. Upwelling longwave radiative heat flux was estimated assuming an emissivity for water of 0.97 with lake surface temperature as measured at 6 m depth. The difference in lake water temperature at observed 3 and 6 m is small (root mean square difference of 0.3 °C over 15 continuous months of simultaneous observation at both depths), suggesting surface waters are typically well mixed (Fig. 2c). Thus, the more complete record of water temperature at 6 m depth was used as a proxy for surface temperature.

Matlab Air-Sea toolbox v2 (Pawlowicz et al., 2001), which applies a simplified version of Fairall et al. (1996) to compute sensible and latent heat fluxes, was applied using observed air temperature, atmospheric pressure and relative humidity.

Long wave radiative, sensible and latent heat fluxes were neglected during periods of complete ice-cover. With no observations near the ice-water interface, we are essentially assuming that heat flux imbalances at the ice-water interface will lead to accretion or melting of ice. As will be shown, a good balance in the heat budget (despite our approximations) supports these decisions and approximations. No attempt was made to account for partial ice-cover, and periods of partial ice-cover were treated as open water for the purposes of estimating all heat fluxes.

2.5. Stratification and mixing dynamics

We quantify strength of density stratification using Schmidt Stability as defined by Idso (1973) as

$$S_t = \frac{g}{A_S}\int_0^H (\rho - \rho_o)(z - z_v)A dz \tag{2}$$

in J m^{-2}. Here, we integrate upwards from the lake bottom at z = 0 to the free surface at z = H (assumed constant), g is gravitation acceleration, $\rho = \rho(z, t)$ is the lake water density, ρ_o is a reference density taken as 1000 kg m^{-3}, A is the lake hypsograph and is a function of elevation (z), and z_v is the elevation of the lake centre of volume.

Surface buoyancy flux (B_o) is separated into penetrative (B_P) and non-penetrative (B_{NP}) components and is estimated from net surface heat flux as

$$B_o = B_P + B_{NP} = \frac{g\alpha}{\rho_o c_p}H_P + \frac{g\alpha}{\rho_o c_p}H_{NP} \tag{3}$$

where α is the thermal expansion coefficient of water, c_p is the specific heat of water, and H_P and H_{NP} are respectively the surface heat flux due to penetrative (i.e. shortwave radiation) and non-penetrative heat flux (i.e. long wave radiation, sensible and latent). The thermal expansion coefficient and specific heat of Nam Co water were calculated using the thermodynamic equation of state (TEOS-10; Pawlowicz and Feistel, 2012), with *in situ* temperature and a nominal salinity of 1.5 g L^{-1}. Note, the thermal expansion coefficient is strongly temperature dependent, crossing zero and changing sign at T_{md}. Nam Co salinity depresses the temperature of maximum density (T_{md}) to 3.65 °C at local atmospheric pressure (note, the increase in T_{md} due to reduced atmospheric pressure at the elevation of Nam Co is negligible). As will be shown, H_P is always net heating (i.e. negative) and H_{NP} is always net cooling at Nam Co. Thus, B_P and B_{NP} will be of opposite sign and whether these buoyancy fluxes stabilize or destabilize the water column will depend on water temperature relative to T_{md}.

In order to classify the various stages of seasonal evolution of thermal stratification we identify stratification phases based on strength of stratification, surface water temperature relative to T_{md}, ice-cover, and heat and mixing dynamics. Following the recommendation of Engelhardt and Kirillin (2014), we use a Schmidt Stability (S_t) threshold to delineate periods of strong stratification from periods of weak stratification. We use a delineation threshold of S_t = 100 J m^{-2}; the same threshold used by Priet-Mahéo et al (2018) who studied summer stratification in a similar depth Arctic lake (Lake Lagerflot, Iceland, maximum depth 110 m, mean depth 42 m). Further classification by surface water temperature relative to T_{md} delineates periods when B_P and B_{NP} are stabilizing or destabilizing the water column. Using these delineations, we classify the seasonal evolution of stratification in Nam Co into six phases whose characteristics we describe in the next section.

To estimate relative importance of wind energy versus buoyancy flux in surface mixed layer energetics, we use Monin-Obukhov depth

$$L_m = \frac{u_*^3}{kB_o} \tag{4}$$

Kundu and Cohen (2008), where k is Von Karman's constant taken as 0.4 and u_* is the wind shear velocity of water estimated using bulk formula for wind stress at the lake surface estimated from wind speed,

$$u_* = \left(\frac{C_D\rho_a}{\rho_o}\right)^{1/2} U \tag{5}$$

with ρ_a the air density taken as 0.73 kg m^{-3} based on mean air pressure and temperature as measured on site, and C_D is a drag coefficient consistent with the elevation above ground of the measured wind speed, U. At depths within the surface mixed layer shallower than L_m, mixing energy by surface wind shear dominates mixing, while at depths within the mixed layer greater than L_m, mixing energy from convection driven by a destabilizing surface buoyancy flux (e.g. due to surface cooling at water temperature greater than T_{md}) dominates mixing. For a stabilizing surface buoyancy flux, L_m is negative, in which case L_m indicates depth to which wind mixing is effective. Wind stress is zero under-ice, which implies L_m = 0.

3. Results

To provide context to water column observations, we begin with a description of observations of atmospheric, lake surface temperature, and snow and ice. This is followed by detailed observations of water state variables (i.e. temperature, dissolved and suspended solids) to show temperature variations dominate buoyancy, expect for a brief period during Spring melt when water temperature approaches T_{md} and dissolved solids become relatively important at a time when stratification is extremely weak. We subsequently present a heat budget to validate estimated heat fluxes, from which surface buoyancy flux is calculated. We then describe the relative importance of wind stirring and buoyancy flux due to penetrating versus non-penetrating heat fluxes.

3.1. Observations of surface conditions

Consistent with You et al. (2007)'s observation of a mean annual temperature of ~0 °C (from 14 July 2005 to 13 July 2006), the mean annual air temperature during the three years of observation was −0.5 °C, with daily average temperature ranging from −20 to 10 °C (Fig. 2c) and daily temperature ranges of up to 20 °C. Daily average air temperature was below 0 °C for 160 ± 32 days each year, with a three-year mean annual minimum temperature of −29 ± 0.5 °C. During winter months (1 November – 30 April) wind speed corrected to 10 m elevation, mean wind speed was 4.4 m s^{-1} and direction consistent from 250°, while during the remainder of the year mean wind speed decreased to 3.6 m s^{-1} and wind direction was more variable (Fig. 2e and f).

Maximum surface water temperature was comparable to maximum daily average air temperature, but with a 38-day lag (Wang et al., 2019), while minimum surface water temperature was close to 0 °C, and annual mean surface temperature was 6.3 °C, almost 7 °C warmer than the mean annual air temperature (Fig. 2c). Air temperature only exceeded surface water temperature for about 6 weeks each year beginning in May (Fig. 2c). The water surface temperatures are abnormally low for a lake at the relatively low latitude of 30° N, indicating the profound effect of high altitude on lake forcing.

Visible satellite imagery indicated, consistent with a predominantly west-southwest wind, ice began to form and accumulate on the eastern shore of the relatively shallow East Basin (e.g. Fig. 3d) at start of freeze up in mid- to late-December (Table 1). Ice-cover then spread westward with the East Basin completely ice-covered by early to mid-January. During the three years of observation, ice-cover was complete on Nam Co by the end of January each year, consistent with Gou et al. (2017). In all monitored years, the annual-average ice-thickness was 0.55 ± 0.1 m. Ice break up occurred in a reverse pattern with leads forming along the western shore around April, then open water spreading eastward. Large ice pans (1–10 km diameter) were observed in the Main Basin, while the East Basin remained completely ice-covered (e.g. Fig. 3d). By mid-May only the East Basin remained ice-covered and by mid- to late-May of each year Nam Co was ice-free (Fig. 3a), consistent with Cai et al. (2019).

Nam Co ice-cover is often free of snow (e.g. Fig. 3b); however, 2–3 substantial snowfall events completely cover the lake each winter (Table 1; e.g. Fig. 3c). These snow-covered periods likely dramatically reduced penetrating shortwave radiation entering the water column (c.a. Bouffard et al., 2019). During the three years observed in this study the total number of days of complete snow cover were relatively low (< 30 days) in 2012 and 2014, while 2013 had over twice the duration of snow cover (69 days; Table 1). As will be shown, this larger number of days of complete snow cover is correlated with a decrease by a factor of two in rate of water column heating.

3.2. Observations of seasonal evolution of stratification

3.2.1. Thermal stratification

Nam Co is dimictic with ~5 months of summer thermal stratification, followed by 1–2 months of near-isothermal conditions during open water, followed by 5–6 months of weak stratification under partial and complete ice-cover (Fig. 4a). As summarized in Table 2, we classify the seasonal evolution of stratification into six phases using the delineations introduced in Section 2.5, and proceed to describe the characteristics of these six phases.

The stratification phases follow the standard seasons of a dimictic lake, i.e. summer, fall turnover, winter, and spring turnover; however, we further separate summer into Summer1, with increasing heat content and stability, and Summer2 with decreasing heat content and stability. As well, we separate fall turnover into Fall1 with water warmer than T_{md} and Fall2 (labelled as "pre-winter" in Kirillin et al., 2012) with water colder than T_{md}, but open-water or partial open-water. This is followed by Winter, with complete ice-cover, then Spring as open-water develops and ice-off proceeds. Nam Co returns to Summer1 as water temperature warms past the temperature of maximum density. Of note, phases Summer1, Summer2, and Fall1 are all at water temperatures warmer than T_{md}, while Fall2, Winter, and Spring are all at water temperatures colder than T_{md}, and only Summer1 and 2 have S_t substantially greater than 100 J m^{-2}. The warm phases (Summer1 and 2, Fall1) are typically observed in warm-monomictic and dimictic lakes, and well documented (e.g. Wetzel, 2001; Spigel et al., 1986), while the cold phases, typical to temperate dimictic lakes, are relatively poorly documented (Kirillin et al, 2012).

Schmidt stability increased rapidly during Summer1 attaining a maximum stratification of ~1700 J m^{-2} in September (Fig. 4b). While this peak S_t is relatively low for temperate lakes, it is higher than the

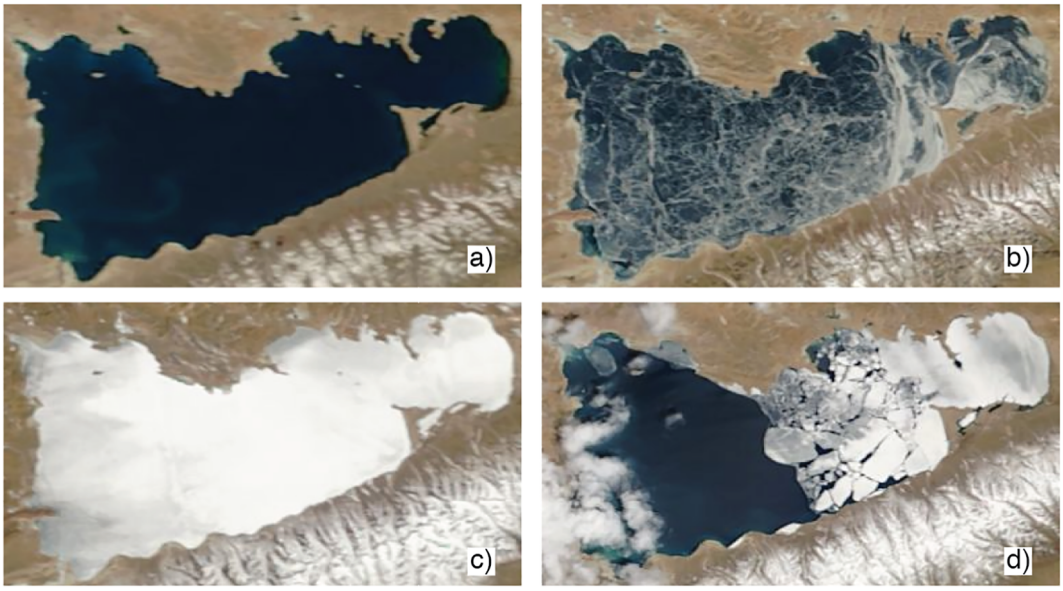

Fig. 3. Satellite images of Nam Co showing various states of ice and snow cover. a) Open water, 20 May 2014. b) Complete ice-cover, no snow, 22 Feb 2012. c) Complete ice and snow cover, 27 Feb 2013. d) Ice coming off with open water in the western half, large ice pans in the eastern half of the Main Basin, and complete ice-cover in the Eastern Basin, 30 April 2014. Images were chosen representative with best quality (i.e. sharpest focus and minimal cloud cover).

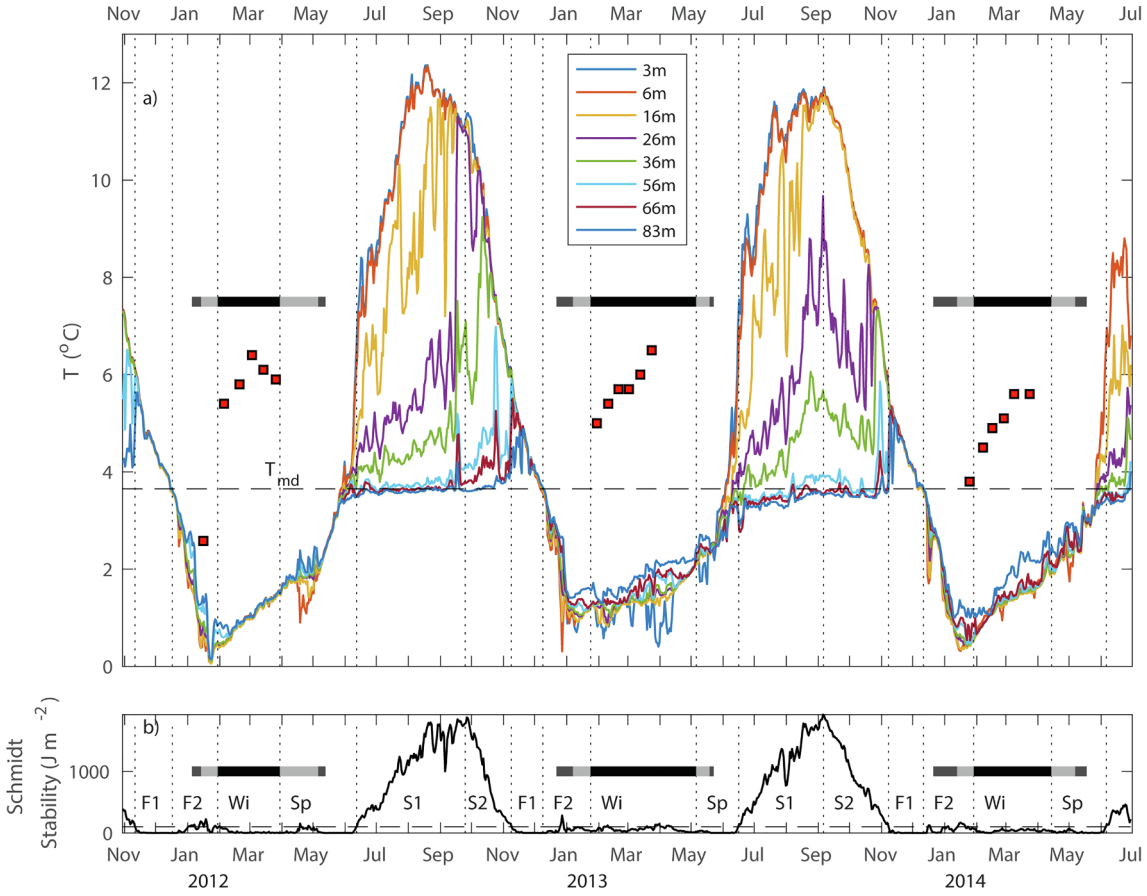

Fig. 4. Thermal stratification dynamics in Nam Co with 6 identified phases of stratification (see Table 2) delineated by vertical dashed lines. a) Water temperature from mooring T2, with horizontal bar indicating stages of ice-cover as dark grey = East Basin partially ice-covered, light grey = East Basin covered and Main Basin partially ice-covered, black = complete ice-cover. The horizontal line is T_{md} at surface pressure based on an absolute salinity of 1.5 g L^{-1}. Ice thickness, in decimetres, is plotted as red squares. b) Schmidt Stability as given by Eq. (2), with labels indicating phases of stratification (see Table 2) delineated by vertical dashed lines.

Table 2
Characteristics of the six identified phases of stratification in Nam Co. Here "weak" stability is defined as $S < 100$ J m^{-2}. Stratification phases Fall2, Winter, and Spring, highlighted in gray, are periods when lake water is colder than T_{md}.

Phase	Lake State				Processes (Fig. 7c-e)		
	T vs T_{md} (Fig. 4a)	Ice cover (Fig. 4a)	Heat content (Fig. 7b)	Stability (Fig. 4b)	Mixing process		Stratifying process
Summer1 (S1)	$T > T_{md}$	None	Increasing	Increasing	surface cooling	+ wind <	penetrative heating
Summer2 (S2)	$T > T_{md}$	None	Decreasing	Decreasing	surface cooling	+ wind >	penetrative heating
Fall1 (F1)	$T > T_{md}$	None	Decreasing	Weak	surface cooling	+ wind >	penetrative heating
Fall2 (F2)	$T < T_{md}$	Partial	Decreasing	Weak	penetrative heating	+ wind ~	surface cooling
Winter (Wi)	$T < T_{md}$	Complete	Increasing	Weak	penetrative heating		insignificant
Spring (Sp)	$T < T_{md}$	Partial	Increasing	Weak	penetrative heating	+ wind >	surface cooling

peak of ~1000 J m^{-2} reported for Lake Lagerflot (Priet-Mahéo et al, 2018). During phase Summer2, the lake cooled rapidly as daily average air temperature fell below 0 °C in late October. This cooling rapidly decreased S_t, transitioning in each of the three observed years from strong to weak stratification in November at a water column temperature of ~5 °C denoting the beginning of Fall turnover (Fall 1). The Fall turnover phases were characterized by cooling with near-zero S_t (i.e. nearly isothermal). During phases Fall1 and Fall2, near-isothermal cooling continued for about 1 month at a rate of 120 ± 20 W m^{-2} averaged over the three years of observation. A minimum water temperature of less than 1 °C occurred during phase Fall2 as ephemeral, weak, inverse stratification developed and broke down, and ice-cover progressed westward across the entire lake.

During the Winter phase, inverse thermal stratification was weak and episodic, especially in 2012 and 2014 though somewhat more persistent in 2013. Nam Co warmed during Winter in all years. During Winter 2012 and 2014 the lake warmed at an average rate of 36 ± 2 W m^{-2}. This was approximately double the 17 W m^{-2} observed during Winter 2013. The reduced under-ice heating observed during Winter 2013 was correlated with significantly increased

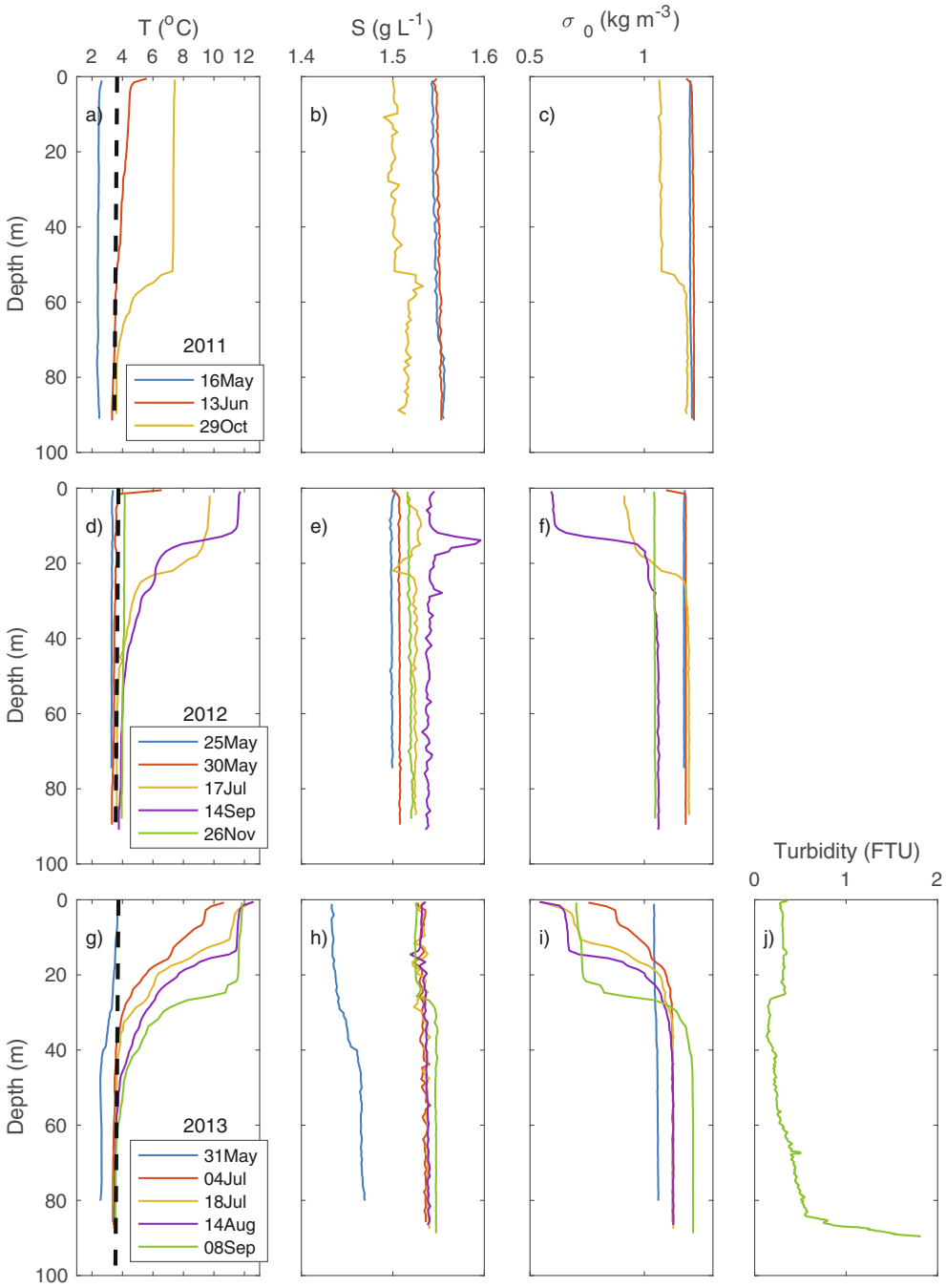

Fig. 5. Vertical profiles of temperature (T), salinity (S) and density (σ_0) at T2 during open water in 2011, 2012, and 2013. The black dashed line is T_{md}. The 8 September 2013 profile was with a Sea & Sun CTD, which included turbidity.

duration of snow cover (Table 1). As will be shown, the calculated rate of lake warming closely matches the estimated shortwave heat flux, confirming the observed heating of Nam Co under ice-cover was primarily due to shortwave radiation penetrating the snow and ice cover.

The Spring phase was a period of continued weak stratification as ice-cover came off and Nam Co became ice free by the end of May (Table 1). During Spring, the water column warmed while remaining weakly stratified until reaching T_{md}, at which point summer thermal stratification developed rapidly and the lake returned to phase Summer1. In Spring 2012, ice came off completely on 13 May 2012. On 25 May 2012, the water column was nearly isothermal (Fig. 5d and Fig. 4a), ~3 weeks after air temperature first became consistently warmer than 0 °C, and by 30 May 2012 the lake was weakly linearly stratified to 90 m, with surface water warming above T_{md} (Fig. 5d). Thereafter surface water warmed rapidly, while bottom water stayed near T_{md} until mid-August (Fig. 5d; July profile) when bottom water gradually warmed as large amplitude baroclinic motions (reversible temperature changes at all depths), likely driven by changes in wind stress, agitated the lake (Fig. 4a).

A similar spring turnover pattern occurred during Spring 2013, except the bottom water remained below T_{md} until in the beginning of fall turnover in November. At that point, the bottom water abruptly warmed (Fig. 4a). A profile with water warmer than T_{md} at the surface and water colder than T_{md} at the bottom is only gravitationally stable if the thermal stratification is compensated for by another stratifying agent such as dissolved (i.e. salinity) or suspended solids. Profiles of salinity (Fig. 5b, e, h) indicate salt stratification was sufficient to compensate for any apparent temperature inversions, especially around

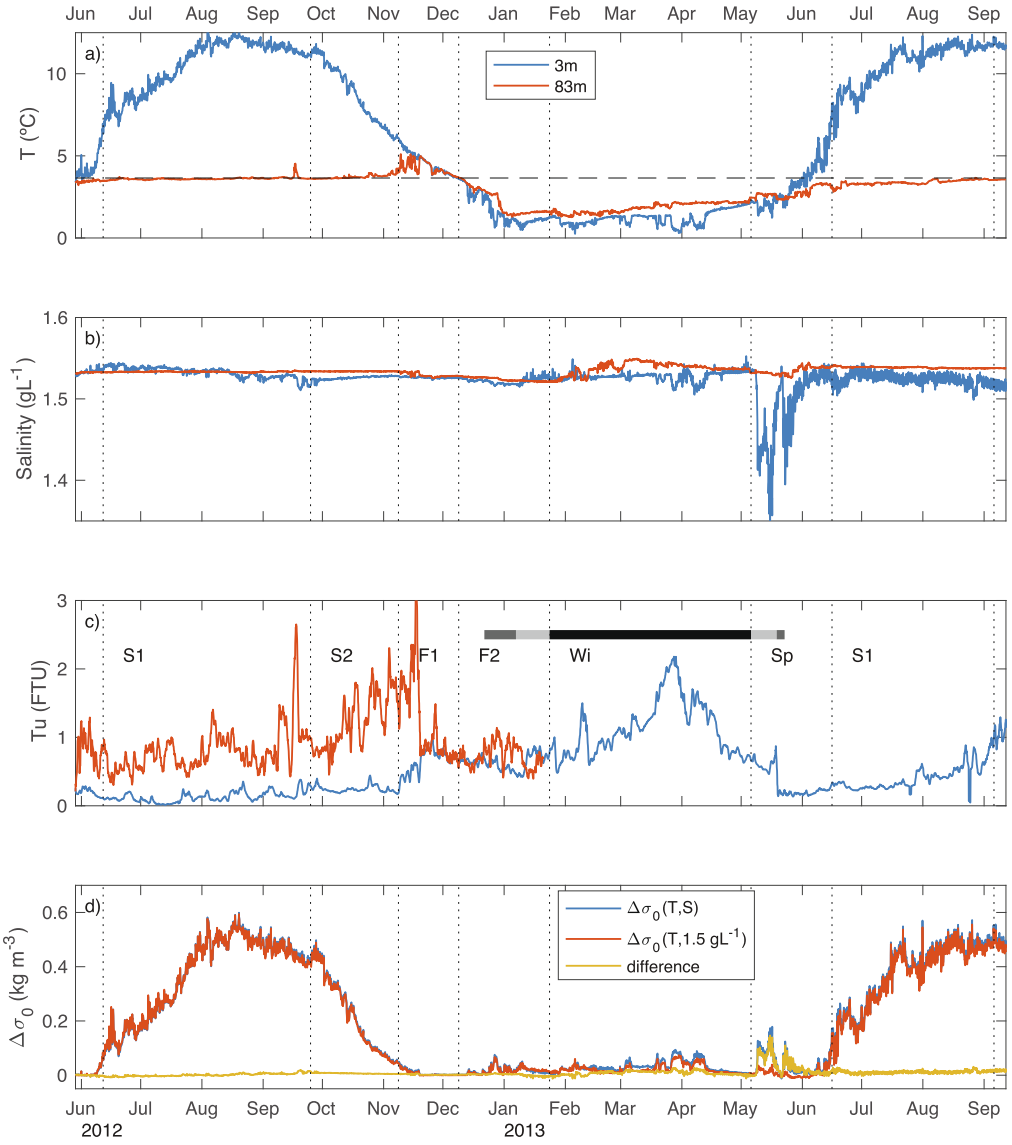

Fig. 6. Seasonal impact of salinity on density as illustrated by time series of state variables as measured by CTD at 3 and 83 m depth at mooring T2. a) Water temperature (horizontal dashed line is T_{md}), b) salinity, c) turbidity, with labels indicating phases of stratification (see Table 2) delineated by vertical dashed lines, and horizontal bar indicating phases of ice cover (as in Fig. 4a). d) Density difference between 83 and 3 m depth estimated using measured temperature and salinity (T, S), measured temperature and a constant salinity (T, 1.5 g L^{-1}) and the difference between those two estimates.

T_{md} where the thermal expansion coefficient approaches zero. This was especially exemplified in May 2013 where the entire water column above 40 m depth was gravitationally unstable if only considering temperature stratification (Fig. 5g). This apparent gravitational instability was compensated by commensurate freshening of the water column at the time of meltwater runoff (Fig. 5h), such that density increased with depth (Fig. 5i).

3.2.2. Dissolved solids

Dissolved ions were generally well-mixed vertically such that salinity is nearly homogeneously distributed in the vertical (Fig. 5b, e, h). The exception to this was during the spring freshet mentioned above (Fig. 5g-i). Seasonal salinity dynamics are further illustrated in time series measured at 3 and 83 m depth at T2 (Fig. 6b). Salinity was relatively constant in time and with depth in all seasons except Spring. There were small fluctuations (~0.02 g L^{-1}) at 3 and 83 m, especially during Winter, and top-to-bottom salinity differences rarely exceeded 0.02 g L^{-1}. However, during Spring, coincident with melting of snow and ice as air temperature increased above zero (Fig. 2c), surface salinity decreased rapidly by ~0.2 g L^{-1}. By the end of Spring, in early June, salinity at 3 m depth had returned to the steady value of ~1.53 g L^{-1} observed during the rest of the year. Thus, temperature dominates over salinity stratification except for a brief period in Spring when the weak stratification was dominated by salinity rather than temperature. This slight freshening of the surface water and commensurate stabilizing of the water column during spring melt are similar to that observed by Pieters and Lawrence (2009) in a small lake (Tailings Lake) with salinity of ~1 g L^{-1}. Though unlike Tailings Lake, this salinity stratification in Nam Co is rapidly broken down before the surface water reaches T_{md}.

Here we quantify the impact of neglecting dissolved solids when calculating S_t (Fig. 4b), by comparing timeseries of density difference between 3 and 83 m using time-varying versus constant (1.5 g L^{-1}) salinity (Fig. 6d). Consistent with CTD profiles discussed above, the impact of assuming a constant salinity was negligible during all phases except Spring, when the salinity stratification was comparatively large (Fig. 6b). During Spring, the temperature stratification was very weak because of small top-to-bottom temperature difference and temperature

near T_{md}, but salinity stratification was relatively strong likely due to melting of snow and ice. Thus, during the Spring phases, salinity likely dominated top-to-bottom density difference, otherwise temperature dominated top-to-bottom density difference.

3.2.3. Suspended solids

Not much is known about suspended solids concentration or turbidity of surface inflows, though visual inspection shows some creeks are glacier fed and hence visibly turbid. Despite this, pelagic turbidity levels at T2 are relatively low. One serendipitous CTD profile at T2 on September 2013 had a turbidity sensor (Fig. 5j). This profile shows generally low turbidity (< 0.5 FTU), except in a bottom layer about 5 m thick where turbidity increased to almost 2 FTU. This observation is consistent with time series of turbidity recorded at 3 and 83 m depth at T2 (Fig. 6c), which in fall of 2012 show ~0.2 and ~1 FTU at 3 m and 83 m respectively. Turbidity at 83 m then increased steadily reaching a peak of ~3 FTU in mid-Fall1 when the lake homogenized in temperature, salinity, and turbidity (Fig. 6a–c). At 3 m, turbidity was below 0.5 FTU until turnover in late November, whereupon it increased to ~1 FTU. Turbidity increased once ice-cover was complete, reaching a maximum of ~2 FTU near the end of March then subsequently decreasing. There was no significant turbidity increase at 3 m during freshet in May/June 2013. These observed low turbidity values suggest suspended solids are not a significant component of stratification away from the near-shore regions.

3.3. Heat budget

Shortwave radiative heating and net longwave radiative cooling dominated the estimated surface heat fluxes at Nam Co (Fig. 7a), especially between ice-off and peak heating (i.e. April through July). Thereafter, cooling due to latent and sensible heat fluxes became progressively more important as shortwave radiative heating decreased. Then, prior to ice formation, there was a very high net cooling of 150–250 W m^{-2}, with latent, sensible and longwave cooling contributing ~100 W m^{-2} each, compared to ~100 W m^{-2} of solar heating. Note that our solar heating estimate uses a long-term average atmospheric transmissivity and neglects short term variations of cloud cover, so this estimate of daily average solar heating does not include daily variability.

As expected during open water, net longwave radiation, and latent heat were always positive (i.e. cooling; Fig. 7a) though notably sensible heat flux was only negative during May-July and at insignificant values (< 10 W m^{-2}). Thus, the open water heat budget was driven by heating due to penetrating shortwave radiation and cooling due to non-penetrating surface heat loss.

Fig. 7b compares the net heat flux into the lake (black line) with the rate of change of heat content within the lake (red line). Conservation of heat requires that these two terms balance. We observe that the two terms agree well, considering the crudeness of the bulk methods used to estimate surface heat fluxes. The balance between these terms is especially good during the cooling phases (Summer2, Fall1 and 2) as well as during the periods of complete ice-cover (Winter); however, the estimated net surface heat flux was ~100 W m^{-2} higher than observed rate of change of heat content during most of Spring and Summer1. The likely cause for this mis-match during Summer1 is the use of a 6 m water temperature as a proxy for surface temperature. During Summer the water column likely develops a diurnal surface layer that is shallower than 6 m and surface temperature is underestimated.

3.4. Energetics of seasonal evolution of thermal stratification

Buoyancy fluxes associated with these surface heat fluxes and wind stirring, change the potential energy of the water column and hence S_t (Fig. 4b). We analyze the seasonal pattern of S_t against the destratifying effects of wind stirring, and the stratifying and destratifying effects of surface buoyancy flux, where we differentiate between penetrating (B_P) and non-penetrating (B_{NP}) components of buoyancy flux.

At seasonal time scales, the rate of change of S_t was dominated by the development and breakdown of seasonal summer stratification during phases Summer1 and 2. During the development of seasonal summer stratification (Summer1) wind power is relatively small (Fig. 7e), while the increase in S_t resulting from solar heating B_P (Fig. 7d) exceeded the mixing produced by wind-stirring and non-penetrative surface cooling B_{NP}, resulting in a net stabilizing buoyancy flux (i.e. $B_o = B_P + B_{NP} > 0$). Conversely, during the break down of seasonal summer stratification (phase Summer2), B_P decreased towards zero, whileB_{NP} continued to become more negative (i.e. $B_o = B_P + B_{NP} < 0$). The resultant available mixing energy was produced more quickly than the development of stratification and the stratification began to break down.

During Summer 2, the seasonal stratification continued to mix until the lake was nearly isothermal, at which time the lake entered Fall1. This phase was characterized by strong wind input while B_o decreased to zero as the water column cooled to T_{md} and α approached zero (Fig. 7d and e). Also, during Fall1, S_t was nearly zero since the lake was nearly isothermal; however, the net rate of input of mixing energy was large, with episodically high u_*. This high wind energy at a time of low B_o and S_t indicates the generated turbulence was primarily being lost to viscous dissipation and there was a low net efficiency.

The continued cooling below T_{md} (phase Fall2) had a variable, but high, rate of wind energy input and low, but stabilizing, B_o. The continued low S_t during Fall2 suggests wind energy input exceeded buoyancy flux.

Once ice-cover was complete (i.e. Winter), there was no wind stress acting on the lake and penetrating solar radiation warmed the water column. The associated negative buoyancy flux (B_o B_P) drove convection, which kept S_t small. Convection may have also be driven by salt rejection during ice formation (c.a. Pieters and Lawrence, 2009). Unfortunately, it is not possible to quantitatively assess this impact since our shallowest thermistor is too deep to resolve the surface thermal boundary layer where water temperatures transitions to the surface boundary condition of 0 °C. However, the small increase of near-bottom salinity (83 m in Fig. 6b) during February may be due to salt rejection as the ice thickness increases. As ice-cover came off during Spring, penetrative solar radiation continued mixing the water column and was aided by relatively weak wind stirring, resulting in weak ephemeral thermal stratification. Thus, the water column remained weakly stratified as it warmed to T_{md}. Despite water temperature being close to T_{md}, B_o was comparable in magnitude but of opposite sign to that in Fall2. Thus, this net positive buoyancy flux during Spring sustained convectively generated turbulence during a period of weak wind (contrary to Fall2 in which wind forcing is strong), and was sufficient to overcome the salinity stratification induced by snow and ice melt. This is contrary to that observed by Pieters and Lawrence (2009) who found salinity stratification induced by spring melt endured until the subsequent fall turnover. Once the water column warms past T_{md}, a rapid increase in buoyancy flux dominated by penetrative solar radiation rapidly stratified the water column with wind stirring developing a shallow mixed layer, and Nam Co entered Summer1.

Note, as mentioned above, that during the Spring phase salinity became a relatively important stratifying agent (Fig. 6d) due to snow and ice melt reducing salinity of the surface waters. However, overall stratification was weak and ephemeral during Spring since both temperature and salinity stratification developed and broke down rapidly and repeatedly (Fig. 6a and b), which is indicative of mixing. Also, salinity anomalies were at times associated with seemingly gravitationally unstable temperature profiles at temperatures below T_{md} (e.g. 31 May 2013 profile in Fig. 5g, h). Thus, salinity stratification was compensatory, resulting in near-neutral density stratification (Fig. 5i).

During Summer 1, the surface mixed layer was shallow and the magnitude of L_m was comparable to or larger than surface layer depth

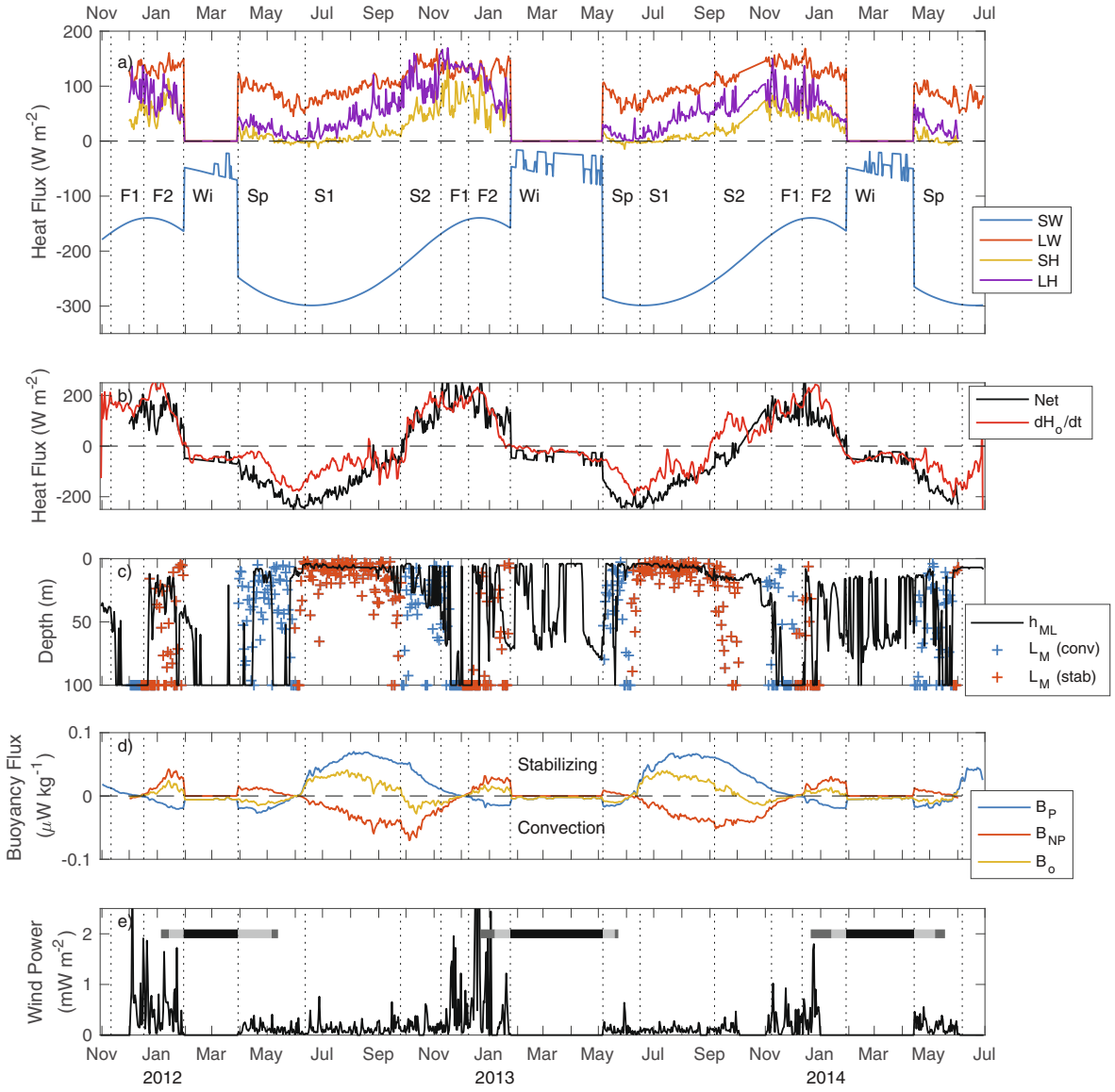

Fig. 7. Water column energetics. a) Estimated heat budget with shortwave radiation (SW), net long wave radiation (LW), sensible heat (SH), and latent heat (LH), with labels indicating phases of stratification (see Table 2) delineated by vertical dashed lines. b) Sum of heat fluxes (Net), and rate of change of Nam Co heat content (dH/dt). While heat fluxes are daily average, dH_o/dt was computed using the difference of daily averages and smoothed with a 30-day running mean. c) Surface mixed layer depth and Monin-Obukhov depth (L_m) colour coded for stabilizing and de-stabilizing net surface buoyancy flux with maximum and minimum values limited to maximum depth of Nam Co. d) Penetrative ($\boldsymbol{B_P}$), non-penetrative ($\boldsymbol{B_{NP}}$) and net ($\boldsymbol{B_o = B_P + B_{NP}}$) buoyancy flux. e) Wind power, showing phases of ice cover as in Fig. 4a.

(Fig. 7c), suggesting mixed layer depth was controlled by wind stirring as would be expected since net buoyancy flux was stabilizing. Progressing into Summer 2, L_m continued to be comparable to or deeper than the surface mixed layer depth suggesting that wind stirring dominated mixing within the deepening surface mixed layer. In contrast, during Fall 1, L_m was often shallower than the mixed layer depth, which consistently encompassed the entire water column, suggesting free convection was maintaining a deep surface mixed layer (Fig. 7c). Because of missing wind data, the only estimates of L_m during Fall2 were associated with net stabilizing B_o, which gave a negative L_m. The magnitude of L_m was comparable or greater than mixed layer depth, suggesting wind stirring dominated within the surface layer. Once ice formed, the surface ice blocked the surface shear stress and $L_m = 0$. As the ice melted (Spring), despite B_o being diminished by water temperature close to T_{md}, L_m was often shallower than the surface mixed layer, suggesting free convection was contributing to a deep surface layer.

4. Discussion

Based on its mictic state, dimictic with 3–5 months of complete ice-cover, Nam Co is similar to other high-latitude, continental lakes such as Great Slave Lake (61° N in Canada) or the Laurentian Great Lakes (40–50° N in Canada and the USA). However, due to its low latitude, Nam Co receives considerably more shortwave radiation; similar to large, warm-monomictic lakes (e.g. Lake Tahoe 2000 m elevation, 39° N in the USA, Sahoo et al., 2016; Lake Biwa, 90 m elevation, 35° N in Japan, Yoshimizu et al., 2010) whose temperatures remain above T_{md} year-round. Thus, the cold climate associated with the high-altitude, relatively low-latitude continental environment of the Tibetan Plateau, results in seasonal thermal stratification similar to that documented for large, high-latitude dimictic lake regions of the world, especially at water temperatures above T_{md} (i.e. Summer1 and 2, and Fall1). However, the arid (i.e. low snow-fall), high-altitude, low-latitude climate of the Tibetan Plateau results in important differences between Nam Co

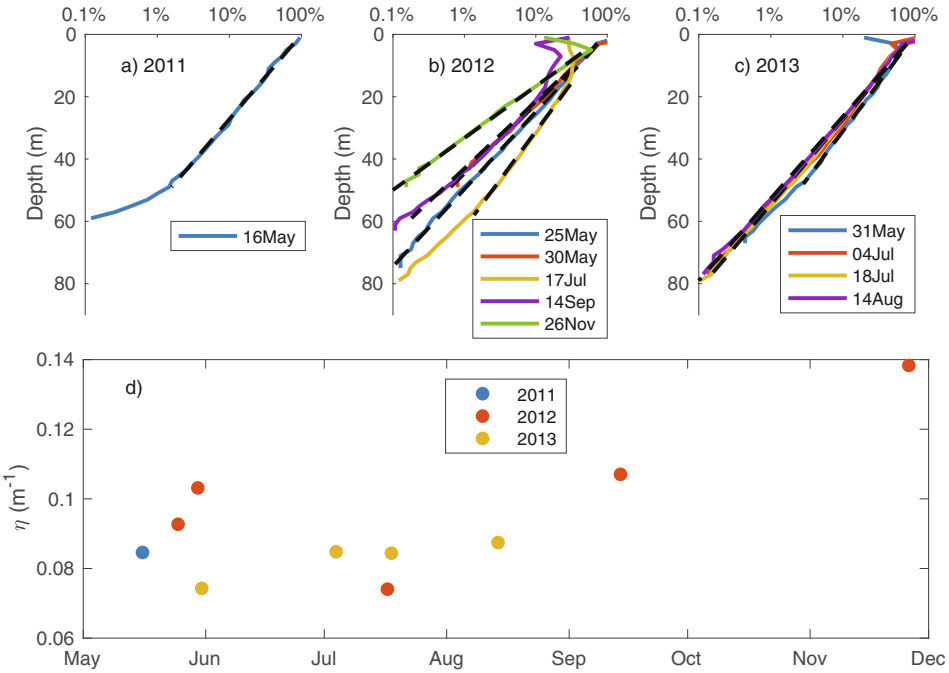

Fig. 8. Optical properties of Nam Co. a) – c) PAR profiles as percent of extrapolated surface value for each year of observation. Linear regressions used to estimate extinction coefficient are over-plotted in black. d) Extinction coefficient estimated from each profile in a) – c).

and similar large, deep high-latitude lakes during the cold phases (i.e. at water temperature below T_{md}) of stratification. We now compare these cold phases of Nam Co with those documented in similar lakes.

Phases Fall1 and 2, encompassing fall turnover, are the periods when the contribution of wind forcing dominates overall mixing, and its destratifying effect generally exceeds any net positive buoyancy flux (Fig. 7c–e). The Fall1 phase in Nam Co was similar to mixing reportedly induced by fall storms at Lake Tahoe, USA (Schladow et al., 2004). Note that Lake Tahoe never cools to T_{md}, and thus never enters Fall2. Net buoyancy flux during Fall2 at Nam Co was relatively low and consistently stabilizing, while wind during Fall2 was strong, keeping Nam Co well stirred, cooling to ~1 °C at 83 m depth before ice-cover was complete. This minimum temperature is lower than observations of Great Slave Lake in which inverse stratification develops at the point where isothermal cooling reaches ~3.5 °C, near their hypolimnetic T_{md} (ca. Schertzer et al., 2003), resulting in no significant Fall2 phase in this high-latitude lake. At the time Great Slave Lake was cooling through T_{md}, net surface heat flux was 200–300 W m^{-2} (note, positive is cooling), which is greater than the 100–200 W m^{-2} estimated for Fall2 in Nam Co. This reduced net cooling due to relatively high solar forcing at Nam Co during fall turnover results in reduced, but positive, buoyancy flux, which is insufficient to negate wind stirring. Thus, the lake remains well-stirred allowing the entire water column to cool prior to complete ice-cover. This cooling of a well-stirred water column to low temperatures in fall is similar to that observed in Lake Superior (47° N), which does not often form complete ice-cover, but does develop a 50–100 m deep surface layer that does cool to below 1 °C, and as low as 0.1 °C in an anomalously cold year (2009) that did form complete ice-cover (Titze and Austin, 2014). While radiatively driven convection helps maintain a well stirred water column during cooling to very low water temperatures in Nam Co, these observations in Lake Superior suggest that in very large lakes, wind stirring can achieve a similar result at high latitude.

Once ice-cover is complete (i.e. Winter), Nam Co begins to gain heat. In their review of winter limnology, Kirillin et al. (2012) discuss under-ice heating of lakes as a late winter process they label “Winter II”. During Winter II the seasonal increase of penetrating shortwave radiation drives convective mixing (Farmer, 1975; Mironov et al., 2002) especially in high latitude regions with large variations in seasonal insolation and persistence of ice-cover almost to summer solstice as snow cover decreases. However, in early winter (i.e. Winter I, see Kirillin et al., 2012) once ice forms, deep, large high-latitude dimictic lakes are observed to continue cooling as inverse thermal stratification develops. For example, under ice-cover Lake Superior cools at 3–124 W m^{-2} until ice comes off and inverse stratification breaks down (Titze and Austin, 2014). In a second example, once ice forms on Great Slave Lake, the lake inversely stratifies, and it continues to cool through the end of December (Schertzer et al., 2003) with net surface heat flux near zero (Rouse et al., 2003). Thereafter, deep water temperatures remain nearly constant until spring turnover in June. Conversely, during the entire period of ice-cover, Nam Co heats at 17–36 W m^{-2} depending on the presence of snow-cover on the ice. Thus, Nam Co does not experience Winter I, rather skipping straight to Winter II (our Winter phase) during the entire period of complete ice-cover. Furthermore, Nam Co water is exceptionally clear with bulk extinction coefficient-based fitting a Beer’s Law exponential relation to open-water, vertical PAR profiles (Fig. 8a-c) ranging between 0.07 and 0.14 m^{-1} (Fig. 8d), corresponding to 1% light levels ranging from 33 to 63 m. This deep penetration of solar radiation will destabilize the water column to great depth likely contributing to low stability throughout the three cold phases.

Similar to observations of high-latitude lakes, intense solar radiation in Spring rapidly warms Nam Co while driving convection until T_{md} is reached. Where Great Slave Lake and Lake Superior cool continuously through fall then under ice-cover in winter such that deep-water temperatures drop to 2–3 °C by ice-off (Schertzer et al., 2003; Titze and Austin, 2014; Austin, 2019), it is interesting to note Nam Co cools to about 1 °C during Fall2, then *warms* continuously during Winter, such that at ice-off hypolimnetic temperature is similar to these large high-latitude lakes. Thus, similar to Great Slave Lake, Spring phase in Nam Co is generally somewhat protracted as the lake must warm from ~2 °C to T_{md}, and similar to Lake Superior (Austin, 2019), convective mixing in Nam Co driven by strong penetrating shortwave radiative forcing keeps the water-column well-stirred during this period of reduced wind.

Interannual variation in duration of snow and ice-cover leads to drastic changes in wintertime heating of the water column in Nam Co.

This effect of snow-cover on shortwave radiation albedo is exemplified by comparing the net rate of heating during 2013 with its relatively prolonged snow cover with the two other observed winters. Winter 2013 had 2.5 to 10 times more days of snow cover resulting in half the seasonal average heating rate. The effects of this reduced heating rate due to snow cover in 2013 were, however, mitigated by a longer period of ice-cover. An earlier start to ice-cover reduced open-water heat loss such that the mean water temperature, when complete ice-cover was established, was warmer in 2013 than in the other two winters observed. Complete ice-cover of Nam Co in 2013 was about 50% longer than in 2012 and 2014, such that despite reduced under-ice heating, water column temperatures as ice-cover came off in 2013 were not markedly different from the other two years. The one exception was the bottom temperature in 2013 stayed below T_{md} until about mid-August, well beyond Spring turnover, which may be due to the relatively short Spring phase because of the extended Winter phase. If reduced hypolimnetic water temperature due to anomalously persistent snow cover is not reset at turnover, there is a potential for interannual impact on thermal stratification. However, the subsequent turnover, in fall, was observed to reset hypolimnetic temperature. Thus, there seems to be some capacity for Nam Co to experience interannual variability of seasonal duration and intensity without commensurate long-term change in hypolimnetic temperature.

5. Conclusions

We have presented a three-year record of thermal stratification in a lake on the Tibetan Plateau and investigated factors controlling its seasonal heat and mixing dynamics. Though Nam Co is a terminal lake with relatively high dissolved solids content (salinity ~1.5 g L^{-1}), salinity is of secondary importance to water column stability except in Spring when Nam Co water is close to T_{md}, and winds are relatively weak. Thus, thermal fluxes control the seasonal evolution of water column stratification, which we classify into six distinct phases (Table 2), three phases are warmer and three are colder than T_{md}. The warmer phases include Summer 1 and 2, with the development and breakdown of seasonal summer thermal stratification. Isothermal cooling characterizes the two Fall phases with the lake transitioning from Fall1 to Fall2 as the lake cools through T_{md} and the opposing effects of penetrative and non-penetrative surface buoyancy flux change sign. During Fall2 Nam Co continues to cool as ice-cover spreads upwind across the lake. Winter is the period of complete ice-cover, characterized by continuous warm, and progresses to the Spring phase as ice-cover recedes in the down wind direction and the lake warms to T_{md}. Once surface waters warm through T_{md}, solar radiation rapidly stratifies the water column and Summer1 begins again.

Penetrating and non-penetrating buoyancy fluxes compete to stratify and destratify the lake, with Summer1 the only period when stratification consistently increases (Table 2) and Summer2 when that stratification breaks down to cooling isothermal conditions in Fall1 as nonpenetrative surface buoyancy flux and wind stirring exceed the waning penetrative buoyancy flux. While relatively cold for its latitude, these warm phases in Nam Co are similar to those in most dimictic lakes. The buoyancy flux associated with penetrating and non-penetrating heat flux changes sign as Nam Co water crosses T_{md}. The relatively intense solar forcing due to low latitude and high altitude contributes to maintaining a well-mixed water column more so than at higher latitude, until the entire water column cools to near freezing as ice-cover spreads upwind across the lake. Once ice-cover is complete, the relatively intense solar forcing combined with clear ice and ephemeral snow cover results in continuous heating and stirring of Nam Co during the period of complete ice-cover (Winter phase). This continuous heating during Winter compensates for the extended cooling during Fall2, resulting in hypolimnetic temperature at Spring turnover similar to that observed in high latitude lakes (e.g. Great Slave Lake) that have no appreciable Fall2 and cool continuously at depth during ice-cover. This understanding of the evolution of seasonal stratification will aid in the interpretation of field observations and the development of lake models to predict the influence of a changing climate and other anthropogenic influences on the many lakes distributed across the Tibetan Plateau.

CRediT authorship contribution statement

Junbo Wang: Conceptualization, Investigation, Data curation, Visualization, Writing - original draft, Project administration, Funding acquisition. **Lei Huang:** Investigation, Data curation, Visualization, Writing - review & editing. **Jianting Ju:** Investigation, Data curation, Writing - review & editing. **Gerhard Daut:** Investigation, Data curation, Project administration, Writing - review & editing. **Qingfeng Ma:** Investigation, Data curation, Writing - review & editing. **Liping Zhu:** Conceptualization, Project administration, Funding acquisition, Supervision, Writing - review & editing. **Torsten Haberzettl:** Project administration, Writing - review & editing. **Jussi Baade:** Project administration, Writing - review & editing. **Roland Mäusbacher:** Project administration, Writing - review & editing, Funding acquisition, Supervision. **Andrew Hamilton:** Methodology, Formal analysis, Writing - review & editing. **Kelly Graves:** Methodology, Formal analysis, Writing - review & editing. **Jason Olsthoorn:** Methodology, Formal analysis, Writing - review & editing. **Bernard E. Laval:** Conceptualization, Methodology, Formal analysis, Visualization, Writing - original draft.

Declaration of Competing Interest

The authors declare that they have no known competing financial interests or personal relationships that could have appeared to influence the work reported in this paper.

Acknowledgments

We are very grateful to Ruimin Yang, Feng Chen, Xing Hu, Jifeng Zhang and Yong Wang for their assistance in the field. Special thanks are given to Shichang Kang, Yaoming Ma and Guoshuai Zhang for providing the meteorological data of the Nam Co research station. Thanks to Dr. Gregory Lawrence whose insights on a later draft of this manuscript helped bring out the key ideas. This work was jointly financed by the Strategic Priority Research Program of Chinese Academy of Sciences (Grant No. XDA20070101) the National Natural Science Foundation of China (Grant Nos. 41877168, 41571189) and the CADY project (TP2:03G0813F) from BMBF, Germany. We acknowledge the use of imagery from the NASA Worldview application (https://worldview.earthdata.nasa.gov/) operated by the NASA/Goddard Space Flight Center Earth Science Data and Information System (ESDIS) project.

Appendix A. Supplementary data

Supplementary data to this article can be found online at https://doi.org/10.1016/j.jhydrol.2020.124668.

References

Austin, J., 2019. Observations of radiatively driven convection in a deep lake. Limnol. Oceanogr. 64, 2152–2160.

Bengsston, L., Malm, J., Terzhevik, A., Petrov, M., Boyarinov, P., Glinsky, A., Palshin, N., 1996. Field investigations of winter thermos- and hydrodynamics in a small Karelian lake. Limnol. Oceanogr. 41 (7), 1502–1513.

Bouffard, D., Zdorovennova, G., Bogdanov, S., Efremova, T., Lavanchy, S., Palshin, N., Terzhevik, A., Vinnå, L.R., Volkov, S., Wüest, A., Zdorovennov, R., Ulloa, H., 2019. Under-ice convection dynamics in a boreal lake. Inland Waters 2, 142–161. https://doi.org/10.1080/20442041.2018.1533356.

Cai, Y., Ke, C.-Q., Li, X., Zhang, G., Duan, Z., Lee, H., 2019. Variations of Lake Ice Phenology on the Tibetan Plateau From 2001 to 2017 Based on MODIS Data. J.

Geophys. Res. Atmos. 124, 825–843.
Engelhardt, C., Kirillin, G., 2014. Criteria for the onset and breakup of summer lake stratification based on routine temperature measurements. Fund. Appl. Limnol. 184 (3), 183–194. https://doi.org/10.1127/1863-9135/2014/0582.
Fairall, C.W., Bradley, E.F., Godfrey, J.S., Wick, G.A., Edson, J.B., Young, G.S., 1996. Cool-skin and warm-layer effects on sea surface temperature. J. Geophys. Res. 101 (C1), 1295–1308. https://doi.org/10.1029/95JC03190.
Farmer, D.M., 1975. Penetrative convection in the absence of mean shear. Q. J. R. Meteorolo. Soc. 101, 869–891.
Farmer, D.M., Carmack, E.C., 1981. Wind mixing and restratification in a lake near the temperature of maximum density. J. Phys. Oceanogr. 11, 1516–1533.
Gou, P., Ye, Q., Che, T., Feng, Q., Ding, B., Lin, C., Zong, J., 2017. Lake ice phenology of Nam Co, Central Tibetan Plateau, China, derived from multiple MODIS data products. J. Great Lakes Res. 43, 989–998.
Guan, Z.H., Chen, C.Y., Ou, Y.X., Fan, Y.Q., Zhang, Y.S., Chen, Z.M., Bao, S.H., Zu, Y.T., He, X.W., Zhang, M.T., 1984. Rivers and Lakes in Tibet. Science Press, Beijing, pp. 1–238 (in Chinese).
Haginoya, S., Fujii, H., Kuwagata, T., Xu, J., Ishigooka, Y., Kang, S., Zhang, Y., 2009. Air-lake interaction features found in heat and water exchanges over Nam Co on the Tibetan Plateau. SOLA 5, 172–175. https://doi.org/10.2151/sola.2009-044.
Hutchison, G.E., Löffler, H., 1956. The thermal classification of lakes. Proc. Nat. Acad. Sci. 42, 84–86.
Idso, S.B., 1973. On the concept of lake stability. Limnol. Oceanogr. 18, 681–683. https://doi.org/10.4319/lo.1973.18.4.0681.
Kirillin, G., Leppäranta, M., Terzhevik, A., Granin, N., Bernhardt, J., Engelhardt, C., Efremova, T., Golosov, S., Palshin, N., Sherstyankin, P., Zdorovennova, G., Zdorovennov, R., 2012. Limnology of seasonally ice-covered lakes: a review. Aquat. Sci. 74 (4), 659–682.
Kundu, P., Cohen, I., 2008. Fluid Mechanics, fourth ed. Academic Press, pp. 872.
Launiainen, J., Cheng, B., 1998. Modelling of ice thermodynamics in natural water bodies. Cold Reg. Sci. Technol. 27, 153–178.
Lazhu, Yang, K., Wang, J., Lei, Y., Chen, Y., Zhu, L., Ding, B., Qin, J., 2016. Quantifying evaporation and its decadal change for Lake Nam Co, central Tibetan Plateau. J. Geophys. Res. Atmos. 121, 7578–7591. https://doi.org/10.1002/2015jd024523.
Lewis Jr., W.M., 1983. A revised classification of lake based on mixing. Can. J. Fish. Aquat. Sci. 40 (10), 1779–1787.
Ma, N., Szilagyi, J., Niu, G., Zhang, Y., Zhang, T., Wang, B., Wu, Y., 2016. Evaporation variability of Nam Co Lake in the Tibetan Plateau and its role in recent rapid lake expansion. J. Hydrol. 537, 27–35. https://doi.org/10.1016/j.jhydrol.2016.03.030.
Ma, Y., Yi, C., Wu, J., Yao, J., 2012. Lake surface expansion of Nam Co during 1970–2009: evidence of satellite remote sensing and cause analysis. J. Glaciolo. Geocryol. 34, 81–88 (in Chinese with English abstract).
MacIntyre, S., Melack, J.M., 2009. Mixing dynamics in lakes across climatic zones. In: Likens, G.E. (ed.) Lake ecosystem ecology. 480 pages.
Mironov, D., Terzhevik, A., Kirillin, G., Jonas, T., Malm, J., Farmer, D., 2002. Radiatively driven convection in ice-covered lakes: observations, scaling, and a mixed-layer model. J. Geophys. Res. Oceans 107 (C4), 3032. https://doi.org/10.1029/2001JC000892.
Pawlowicz, R., 2008. Calculating the conductivity of natural waters. Limnol. Oceanogr.: Methods 6, 489–501.
Pawlowicz, R., Feistel, R., 2012. Limnological applications of the thermodynamic equation of seawater 2010 (TEOS-10. Limnol. Oceanogr. Methods 10, 853–867. https://doi.org/10.4319/lom.2012.10.853.
Pawlowicz, R., Beardsley, R., Lentz, S., Dever, E., Anis, A., 2001. Software simplifies air-sea data estimates. EOS Trans. Am. Geophys. Union 82 (1). https://doi.org/10.1029/01EO00004. 2-2.
Payne, R.E., 1972. Albedo of the Sea surface. J. Atmos. Sci. 29, 959–970.
Peixoto, J.P., Oort, A.H., 1992. Physics of Climate 520.
Perovich, D.K., 1991. Seasonal changes in sea-ice optical properties during fall freeze-up. Cold Reg. Sci. Technol. 19, 261–273.
Pieters, R., Lawrence, G., 2009. Effect of salt exclusion from lake ice on seasonal circulation. Limnol. Oceanogr. 54, 401–412.
Priet-Mahéo, M.C., Ramón, C.L., Rueda, F.J., Andradóttir, H.Ó., 2018. Mixing and internal dynamics of a medium-size and deep lake near the Arctic Circle. Limnol. Oceanogr. 64, 1–20. https://doi.org/10.1002/lno.11019.
Qiu, J., 2008. China: the third pole. Nature 454, 393–396.
Rouse, W.R., Oswald, C.M., Binyamin, J., Blanken, P.D., Schertzer, W.M., Spence, C., 2003. Interannual and seasonal variability of the surface energy balance and temperature of central Great Slave Lake. J. Hydrometeorol. 4, 720–730.
Sahoo, G.B., Forrest, A.L., Schladow, S.G., Reuter, J.E., Coats, R., Dettinger, M., 2016. Climate change impacts on lake thermal dynamics and ecosystem vulnerabilities. Limnol. Oceanogr. 62 (2), 496–507.
Schertzer, W.M., Rouse, W.R., Blanken, P.D., Walker, A.E., 2003. Over-lake meteorology and estimated bulk heat exchange of Great Slave Lake in 1998 and 1999. J. Hydrometeorol. 4, 649–659.
Schladow, S.G., Palmarsson, S.O., Steissberg, T.E., Hook, S.J., 2004. An extraordinary upwelling event in a deep thermally stratified lake. Geophys. Res. Lett. 31, L15504. https://doi.org/10.1029/2004GL020392.
Spigel, R.H., Imberger, J., Rayner, K.N., 1986. Modeling the diurnal mixed layer. Limnol. Oceanogr. 31, 533–556.
Swinbank, W.C., 1963. Long-wave radiation from clear skies. Q. J. R. Meteorolo. Soc. 89 (381), 339–348.
Titze, D.J., Austin, J.A., 2014. Winter thermal structure of Lake Superior. Limnol. Oceanogr. 59 (4), 1335–1348.
Wang, M., Hou, J., Lei, Y., 2014. Classification of Tibetan lakes based on variations in seasonal lake water temperature. Chin. Sci. Bull. 59, 4487–4855.
Wang, J., Zhu, L., Daut, G., Ju, J., Lin, X., Wang, Y., Zhen, X., 2009. Investigation of bathymetry and water quality of Lake Nam Co, the largest lake on the central Tibetan Plateau, China. Limnology 10, 149–158.
Wang, J., Zhu, L., Wang, Y., Ju, J., Xie, M., Daut, G., 2010. Comparisons between the chemical compositions of lake water, inflowing river water, and the lake sediment in Nam Co, central Tibetan Plateau, China and their controlling mechanisms. J. Great Lakes Res. 36, 587–595.
Wang, J., Huang, L., Ju, J., Daut, G., Wang, Y., Ma, Q., Zhu, L., Haberzettl, T., Baade, J., Mäusbacher, R., 2019. Spatial and temporal variations in water temperature in a high- altitude deep dimictic mountain lake (Nam Co), central Tibetan Plateau. J. Great Lakes Res. 45, 212–223.
Wetzel, R.G., 2001. In: Limnology: Lake and River Ecosystems, third ed. Academic Press, San Diego California, pp. 1006.
Yoshimizu, C., Yoshiyama, K., Tayasu, I., Koitabashi, T., Nagata, T., 2010. Vulnerability of a large monomictic lake (Lake Biwa) to warm winter event. Limnology 11, 233–239. https://doi.org/10.1007/s10201-009-0307-3.
You, Q., Kang, S., Li, C., Li, M., Liu, J., 2007. Variation features of meteorological elements at Nam Co station, Tibetan Plateau. Meteorol. Monthly 33, 54–60 (in Chinese with English abstract).
Zhang, G., Yao, T., Xie, H., Kang, S., Lei, Y., 2013. Increased mass over the Tibetan Plateau: from lakes or glaciers? Geophys. Res. Lett. 40, 2125–2130.
Zhou, S., Kang, S., Chen, F., Joswiak, D.R., 2013. Water balance observations reveal significant subsurface water seepage from Lake Nam Co, south-central Tibetan Plateau. J. Hydrol. 491, 89–99.
Zhu, L., Xie, M., Wu, Y., 2010. Quantitative analyses of lake area variations and the influence factors from 1971 to 2004 in the Nam Co Basin of the Tibetan Plateau. Chin. Sci. Bull. 55, 1294–1303.